The Astrophysical Journal Letters, 908:L13 (11pp), 2021 February 10 https://doi.org/10.3847/2041-8213/abd93e

Imaging Titan's Organic Haze at Atomic Scale

Fabian Schulz[1,4,5], Julien Maillard[2,3,4], Katharina Kaiser[1], Isabelle Schmitz-Afonso[3], Thomas Gautier[2], Carlos Afonso[3], Nathalie Carrasco[2], and Leo Gross[1]
[1] IBM Research—Zurich, 8003 Rüschlikon, Switzerland
[2] Université Paris-Saclay, UVSQ, CNRS, LATMOS, 78280, Guyancourt, France
[3] Normandie Univ, COBRA UMR 6014 et FR 3038 Univ Rouen; INSA Rouen; CNRS IRCOF, 1 Rue Tesnière, 76821 Mont-Saint-Aignan Cedex France
Received 2020 October 21; revised 2021 January 5; accepted 2021 January 5; published 2021 February 12

Abstract

Titan, Saturn's largest moon, has its atmosphere filled with a thick organic photochemical haze. These suspended solid nanoparticles are one of the most complex organic materials in the Solar System. In situ measurements from the successful Cassini space mission gave first clues on the aerosol's chemical composition: pyrolysis coupled to mass spectrometry revealed a nitrogen-rich core, whereas infrared measurements highlighted poly-aromatic-hydrocarbon (PAH) signatures. The combination of these observations supports a general model of nitrogenated-polycyclic aromatic hydrocarbon (N-PAH). To constrain the generic picture and understand the formation of such macromolecules in Titan's atmosphere, we simulated the haze synthesis in the laboratory. Small (3–10 rings) N-PAH molecules composing the material were extracted, focusing on the prime aromatization and growth processes. By high-resolution atomic force microscopy (AFM), we imaged key chemical structures with atomic resolution. We resolved N-rich elongated molecules involving five-membered aromatic rings, consistent with a repetitive *cata*-condensation pattern via addition of C_3N units. These atomic-scale observations bridge the gap between gas phase atmospheric reactants and the macroscopic structure of Titan's haze.

Unified Astronomy Thesaurus concepts: Pre-biotic astrochemistry (2079)

1. Introduction

Titan is an organic world, surrounded with thick haze layers produced from atmospheric photochemistry coupling N_2 and CH_4 (Atreya 2007). On the early Earth 2.8 Gyr ago, before the rise of oxygen, biological methane was accumulating in the atmosphere, leading to large concentrations of methane in the atmosphere. At that time, haze was likely formed on the early Earth according to similar processes as on Titan (Pavlov et al. 2001), providing a highly concentrated source of organic material that might have helped evolution of life on the early Earth. Therefore, studying Titan today gives us insight about the atmospheric processes leading to organic haze on early Earth before the rise of oxygen (Trainer et al. 2006).

The Titan haze presents a high degree of chemical complexity that is slowly unraveled through the direct observations made by the successful Cassini-Huygens mission (Coates et al. 2007; Israël et al. 2005; Vinatier et al. 2012; Waite et al. 2007) and the reproduction of the chemical processes in the laboratory with experimental simulations (Coll et al. 2013; Gautier et al. 2017; He et al. 2017; He & Smith 2014; Imanaka et al. 2004; Sciamma-O'Brien et al. 2014; Szopa et al. 2006). Poly-aromatic-hydrocarbon (PAH) signatures were detected in Titan's haze based on the onboarded Visual and Infrared Mapping Spectrometer (VIMS; Dinelli et al. 2013; Gautier et al. 2017; López-Puertas et al. 2013; Yoon et al. 2014). These signatures are compatible with N-PAH molecules, in agreement with the N-rich core reported by the Aerosol Collector and Pyrolyser (ACP) instrument (Israël et al. 2005). Nitrogen is an important element in prebiotic chemistry, as revealed in amino acids or N-rich DNA bases. The radiative impact of N-rich materials is also expected to be significant because N-rich aerosols are efficient ultraviolet (UV) absorbers (Mahjoub et al. 2012). Concerning Titan's haze analogs synthesized in the present work, referred to as tholins, previous analysis has already suggested the presence of at least small aromatic signatures in the material: Two-Step Laser Desorption Ionization Time-of-Flight Mass Spectrometry highlighted the presence of small aromatics with one to three aromatic rings, with or without nitrogen (Mahjoub et al. 2016). Global analytical techniques gave an overview of the overall structure of the material. Solid-phase NMR showed that tholins' structure is mainly based on unsaturated C = N bonds such as imines or triazine units (Derenne et al. 2012) and ion mobility highlighted a global structure with a slightly higher double-bond equivalent (DBE) than PAH, more in agreement with a nitrogenated PAH (N-PAH) global structure (Derenne et al. 2012; Maillard et al. 2020).

However, the intermediate scale remains missing: how does the organic material grow chemically from one or two aromatic rings toward a large PAH and/or an N-PAH structure? What are the key structures comprising this complex material? The present work, mimicking the growth process in the laboratory and imaging directly intermediate key structures composing the material, gives insights on these open questions.

2. Results

In recent years, atomic force microscopy (AFM) with functionalized tips (Gross et al. 2009) has emerged as a new tool to study complex molecular mixtures. Functionalizing an AFM tip with a carbon monoxide (CO) molecule allows for molecules to be imaged with atomic resolution (Gross et al. 2009;

[4] These authors contributed equally.
[5] Fritz Haber Institute of the Max Planck Society, 14195 Berlin, Germany.

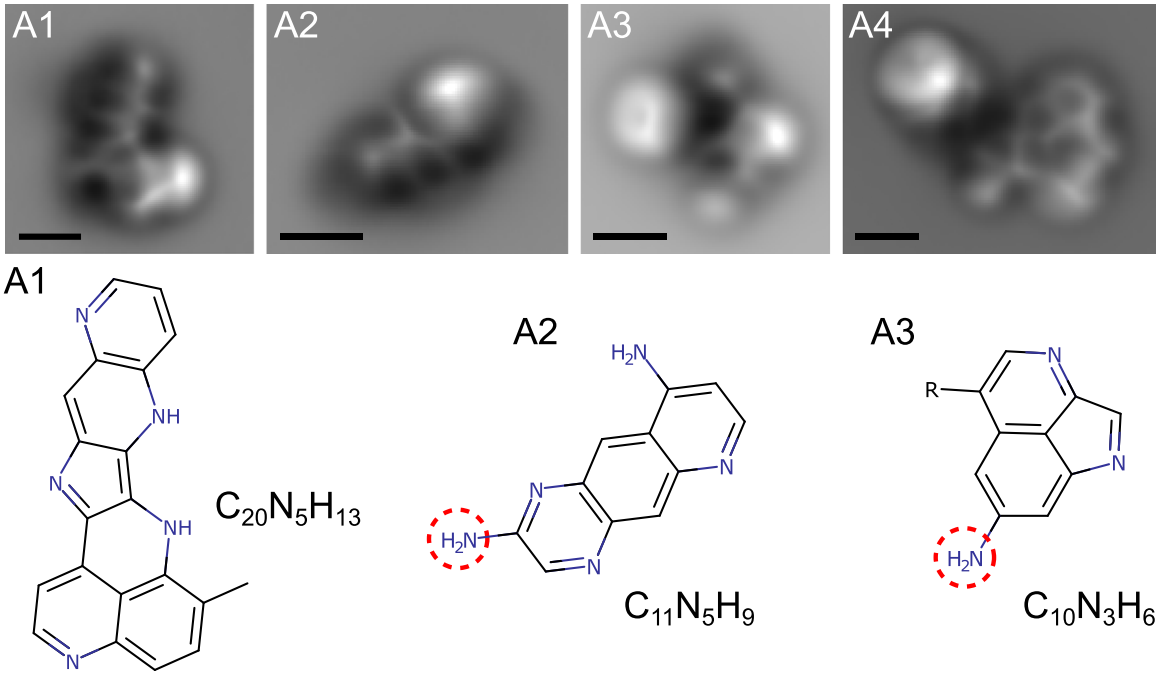

Figure 1. High-resolution AFM images and assigned structures of tholins from the common fraction. All scale bars are 5 Ångström. Red dashed circles indicate uncertain moieties. A possible alternative assignment for the uncertain -NH_2 group in A2, A3 is a -CN group. Additional data obtained on the same molecules is presented in Figure A4 in the Appendix.

Moll et al. 2010) and a priori unknown molecules to be identified (de Oteyza et al. 2013; Gross et al. 2010; Schuler et al. 2015). Here, we employ AFM with CO-functionalized tips to study Titan's haze analogs based on individually resolved molecules.

For AFM analysis, the molecules were sublimed at low temperatures onto a Cu(111) single crystal partially covered by bilayer, (100)-oriented NaCl islands [denoted as NaCl(2ML)/Cu(111)] (see Section 4, and Figure A1 in the Appendix for typical overview image). Based on their solubility in methanol, tholins, i.e., Titan's haze analogs, can be separated into a soluble and an insoluble fraction. We first studied the common fraction containing all molecules (in the following denoted by "A") but found only very few molecules for which atomic resolution could be achieved by AFM; see Figure 1.

In a second set of measurements we studied the insoluble fraction (in the following denoted by "B"), which contained a much larger share of molecules that could be resolved by AFM, see Figure 2. We ascribe this difference to a larger amount of chain-like linker structures in the common fraction compared to the insoluble one (Maillard et al. 2018). In total, around 110 individual molecules were analyzed by AFM. The majority of those were either too bulky, i.e., three-dimensional structures, or too mobile to achieve sufficient atomic resolution to assign their chemical structure. For ∼12% of the analyzed molecules, we were able to propose either their entire chemical structure or at least significant parts of it.

High-resolution AFM is excellently suited to image and identify the structure of planar PAH molecules (Gross et al. 2018). For complex molecular mixtures studied previously, the comparison of AFM-identified molecular structures with mass spectrometry data showed the representativeness of the AFM measurements (Schuler et al. 2017a; Zhang et al. 2018). The AFM technique is best suited for resolving planar structures in the range of about three to about 20 rings. This approximate size window is a result of the preparation method used. The molecules are sublimed by resistive flash heating from a piece of oxidized silicon wafer in ultra-high vacuum (UHV) (Schuler et al. 2015, 2020) onto the sample held at $T = 10$ K. Some of the small molecules (about two rings and less) are too volatile and thus might leave the wafer before the evaporation step. On the other side, large molecules (about 20 rings and more) tend to fragment before their sublimation. The flash heating technique enhances volatility by favoring evaporation and suppressing competitive fragmentation, demonstrated for various compounds (Beuhler et al. 1974; Rapenne et al. 2006). Three-dimensional, highly non-planar molecules are challenging to resolve, as the AFM technique is extremely surface sensitive and only explores the topmost layer of atoms of a surface or a molecule. Thus bulky, three-dimensional molecules that contain more than a single layer of atoms are neglected from our analysis. In addition, some molecules, presumably mainly small ones containing few atoms, are very mobile on the surface, i.e., they are displaced by the AFM tip when attempting to resolve them with atomic resolution, which requires entering the regime of repulsive interaction forces between tip and molecule (Moll et al. 2010). These mobile molecules cannot be resolved and are also neglected from our analysis.

Elemental sensitivity in AFM remains challenging, as the AFM contrast is often a convolution of chemical and topographic information. To obtain a foundation for the structural identification of N-PAH by AFM, we studied several known model compounds featuring different nitrogen-containing moieties (see Figure A2 in the Appendix). In general, we find that the N-containing moieties interact strongly with the underlying substrate's surface, often resulting in slightly non-planar adsorption geometries. These can be resolved with AFM with atomic resolution; the non-planarity only affects the contrast. Moreover, the presence of N atoms within heterocycles leads to distortions in the AFM images as well as subtle contrast variations along the molecular backbone (Ellner et al. 2017; Kocic et al. 2016). For a detailed description of the

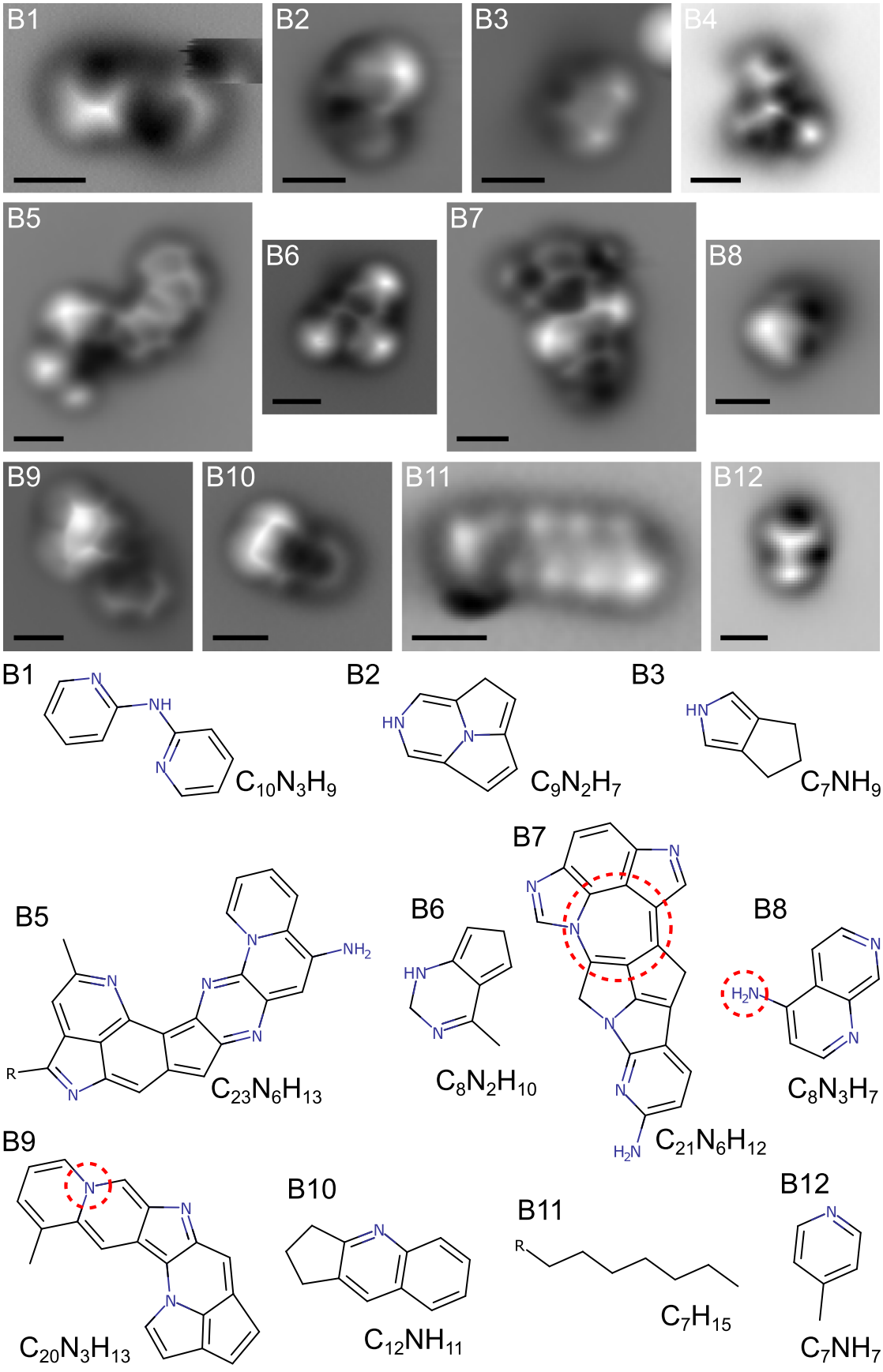

Figure 2. High-resolution AFM images and assigned structures of tholins from the insoluble fraction. All scale bars are 5 Ångström. Red dashed circles indicate uncertain moieties. A possible alternative assignment for the uncertain -NH_2 group in B8 is a -CN group. Additional data obtained on the same molecules is presented in the Figures A4 and A5 in the Appendix.

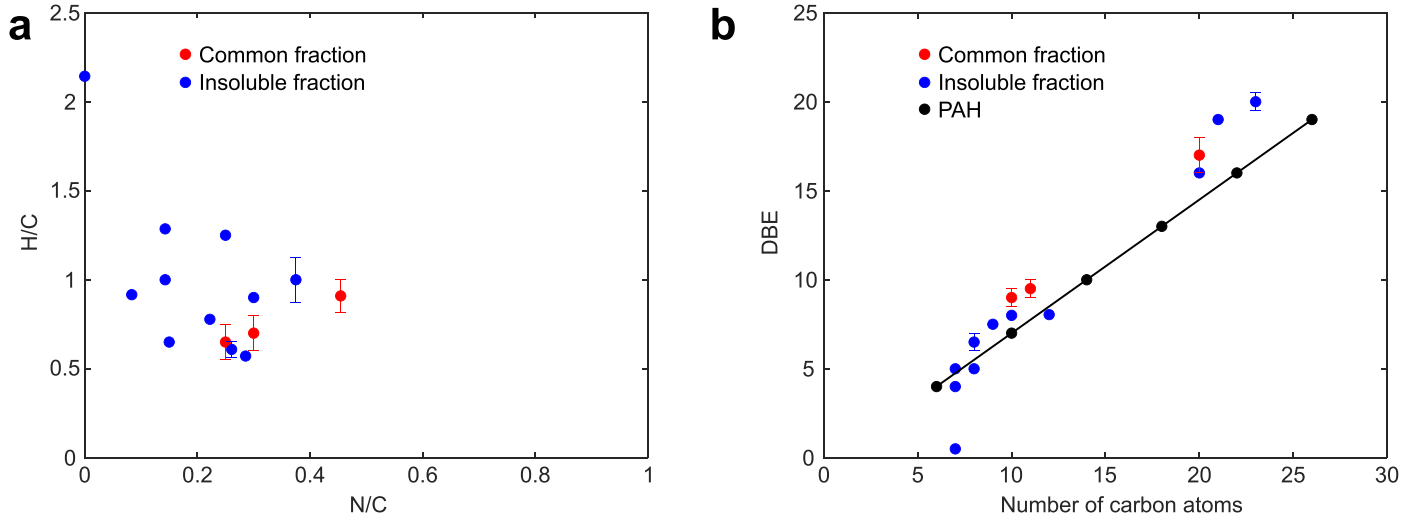

Figure 3. Quantitative analysis of assigned molecular formulas. (a) H/C ratio over N/C ratio. (b) DBE over number of carbon atoms. In (b), the corresponding DBE values for linearly fused (*cata*-condensed) benzenoid PAH are shown as well for comparison. Unassigned parts of molecules denoted as "R" in the proposed structures are neglected. Error bars correspond to the different possibilities of assigning N and NH for some of the structures (see Figure A3 in the Appendix and Supporting Discussion).

characterization of the N-PAH model compounds and discussion of the observed AFM contrast, see the Appendix.

AFM images of atomically resolved molecules are presented in Figures 1 and 2. The assignment of the structures is based on the AFM data shown in the figure, but also on scanning tunneling microscopy (STM) data, and additional AFM data of different height obtained on the same molecules. These additional data, i.e., STM and AFM data at different tip heights on the same molecules, are shown in Figures A4 and A5 in the Appendix. The AFM images show a map of the frequency shift of the oscillating cantilever as the tip is scanned at constant height over the molecule (see Section 4). The molecular structure reveals itself as a bright modulation (more repulsive forces) on top of a dark background (more attractive). Our AFM data show several cyclic or polycyclic molecules. We found molecules containing only one or two cyclic units, e.g., B6 and B12, as well as larger ones, with up to at least seven cyclic units, e.g., A1 and B5. The intensity variations of the AFM contrast along the molecular backbones suggest non-planar adsorption geometries as well as the incorporation of heteroatoms and aliphatic moieties. Molecules containing aliphatic chains or linker structures were also observed; see B1 and B11. In addition, A4 and B4 are examples of molecules for which the AFM images indicate the presence of cyclic units, but strong distortions in the image contrast or strongly repulsive features do not permit inferring the molecule's structure. We assign these distortions to significant non-planarity of the molecule and how it affects the tilting of the CO at the tip apex (Gross et al. 2012; Pavliček et al. 2012; Hamalainen et al. 2014; Hapala et al. 2014). Our assignment of Titan's haze analogs is based on the AFM measurements of the model compounds and previously published AFM studies (Kawai et al. 2018; Kocic et al. 2016; van der Heijden et al. 2016; Schuler et al. 2017b; Zahl & Zhang 2019). In addition, comparison with high-resolution mass spectrometry (HR-MS) data (Ruger et al. 2019) is used to qualitatively confirm the AFM-based molecular structures. In the future, the application of machine learning to interpret AFM images might improve the interpretation and structure assignment of non-planar molecules, including non-PAH structures and heteroatoms (Alldritt et al. 2020).

Figures 1 and 2 show the proposed chemical structures for the imaged molecules, with exception of A4 and B4, which are examples of molecules on which high AFM resolution was obtained, but nevertheless the structure of the molecule remained ambiguous. The assigned structures indicate the frequent occurrence of five-membered rings, either with (e.g., A3, B9) or without N (e.g., B5, B6) as well as partially aliphatic rings (e.g., B3, B10). Another observation from the proposed structures is the elongated shape of the larger molecules (e.g., A1, B5), indicating the frequent occurrence of *cata*-condensation during the formation of N-PAHs in Titan's haze analogs. *Cata*-condensation results in structures in which no more than two rings have a single carbon atom in common. A possible alternative assignment for the uncertain -NH_2 groups in A2, A3 and B8 is a -CN (cyano) group (Fatayer et al. 2019). The finding of the molecule B11 was unexpected and is assumed as a washing contaminant (heptane).

A quantitative analysis of the proposed structures is presented in Figure 3, where we plot H/C over N/C (Figure 3(a)) as well as double-bond equivalent (DBE) over the number of carbon atoms (Figure 3(b)) for each proposed molecular structure. The range of H/C values from our AFM study agrees well with a recent HR-MS study carried out on a comparable mixture of Titan's haze analogs (Ruger et al. 2019), with most molecules having values between 0.5 and 1.5. Surprisingly, the largest N/C within the molecules identified by AFM is just under 0.5, while HR-MS found that a large portion of tholins have N/C values between 0.5 and 1.0. Studying adenine as a nitrogen-rich model compound (Figure A2 in the Appendix), we found that an increased number of nitrogen atoms can result in a complex adsorption behavior with significant non-planarity and strong distortions in the AFM contrast. This renders it challenging to achieve atomic resolution on molecules with higher N content and assign their structure. A possible example for such molecules is B4. This suggests an inherent measurement bias in our AFM study toward molecules with lower N/C ratios. In addition, previous AFM studies (van der Heijden et al. 2016) indicate that N atoms embedded in the polycyclic structure and bonded to three carbon atoms are particularly difficult to differentiate from C atoms, based purely on AFM images. Thus, our proposed chemical structures are more likely to underestimate rather than overestimate the amount of nitrogen atoms.

The DBE *versus* carbon number plotted in Figure 3(b) is a measure of the degree of unsaturation for a given molecular formula. Most of the proposed structures for the insoluble fraction are above the PAH line, indicating their higher degree of unsaturation, in agreement with previous HR-MS results (Maillard et al. 2018).

While our results are not representative for the global properties of tholins, they provide unique insight into the presence and structure of PAH in Titan's haze analogs. Our AFM measurements demonstrate unequivocally that (N-)PAH are part of Titan's haze analogs. Even though quantifying their overall abundance in the sample based on our data is difficult, several additional conclusions can be drawn from our results, as discussed in the following paragraphs.

3. Discussion

Mostly nitrogen-rich structures were observed, orienting the scenario toward N-PAH structures, also in agreement with VIMS measurements on Titan. Several reports have shown evidence for such structures (Derenne et al. 2012; Gautier et al. 2016, 2017; Imanaka et al. 2004). Molecules B3, B12, and B8 are very close to structures identified in previous solid-state NMR analyses (He & Smith 2014; McGuigan et al. 2006). Structures such as A1, B5, and B9 were hypothesized in recent works (Maillard et al. 2020; Ruger et al. 2019). Furthermore, as stated above, the observed structures could contain even more nitrogen atoms that are not revealed because of their pronounced no-planarity.

The other information suggested by our results concerns the formation of this Titan haze analog. We observe that relatively small detected molecules, i.e., 2- to 3-ring structures, such as B3, B6, and B10 contain non-aromatic moieties. In opposition, larger ones such as A1, B5 and B9, i.e., 6- and 7-ring structures, are fully conjugated. The production of this haze is initialized by the formation of small molecules followed by their growth by ion-molecule chemistry (Vuitton et al. 2006; Lavvas et al. 2013). Thus, detected small molecules can be attributed to precursors for larger ones. The molecule B1 is interesting because its structure suggests that if the synthesis conditions had been maintained, molecular growth might have proceeded by a cyclization reaction. Capturing molecules pertaining to different stages of the molecular growth analogously to the conditions in Titan's actual haze, enables novel insights into the growth process.

For pure PAH, *cata*-condensation can be associated with the addition of a C_4 unit (net gain of C_4H_2) and *peri*-condensation with the addition of a C_2 or C_6 unit (net gain of C_2 and C_6H_2, respectively; Hsu et al. 2011). Accordingly, one potential pathway for the growth of N-PAH could be by addition of C_3N or CN and C_5N units. For the structures identified by AFM, there appears to be a prevalence for the addition of C_3N units over CN and C_5N units. Whether this would be due to the relative abundances of the various building blocks or different rate constant for the addition reactions cannot be inferred from our experiments. Prevalent growth via addition of C_3N units would also agree with the plot in Figure 3(a), which reveals the clustering of N/C values around 0.3.

In conclusion, we imaged with atomic resolution individual Titan's haze laboratory analogs and resolved characteristic structural elements such as nitrogen-containing polycyclic aromatic hydrocarbons and elongated N-PAH containing five-membered aromatic rings. This chemical structure is important in several aspects, as it will participate to govern the physical properties of the haze particles in the atmosphere and later at the surface. These molecules are for example good UV absorbers and thus modulate the radiative balance of the atmosphere (Brassé et al. 2015). This chemical structure would also influence the surface energy of the haze particles, controlling their wettability with liquid/solid hydrocarbons and nitriles: it would impact their propensity to trigger methane rains in the troposphere and/or to transiently float at the lake surfaces of Titan (Cordier & Carrasco 2019; Yu et al. 2020). More generally this work showed the potential of AFM technique to reveal the chemical structure of complex organic material of interest for astrochemistry, opening new perspectives in the chemical analysis of rare and complex material such as organic matter contained in meteorites or in the frame of future sample return missions.

4. Methods

Details on the tholins synthesis: Titan's aerosol analogs were produced with the PAMPRE experiment following the same procedure detailed in previous publications (Gautier et al. 2011; Szopa et al. 2006). The reactor is composed of a stainless-steel cylindrical reactor in which a RF-CCP discharge is established thanks to an RF 13.56 MHz frequency generator. A N_2:CH_4 95:5% gas mixture is injected in the chamber as a continuous flow through polarized electrodes and is then extracted by a primary vacuum pump to ensure that gases are homogeneously distributed. The plasma discharge is maintained at a pressure of 0.9 ± 0.1 mbar and at room temperature. A brown powder is recovered after few hours. It should be noticed that the pressure and temperature are lower in Titan's ionosphere (respectively $\sim 10^{-5}$–10^{-8} mbar and 200 K) than in our experiment, but the ionization rate is the same ($\sim ppm_v$). As ion-molecule reaction rates are relatively insensitive to the temperature, the lower temperature in Titan's ionosphere (200 K instead of 293 K in the laboratory) is not an important issue in our case. The higher pressure ensures a faster kinetics in the experiment and is low enough to limit termolecular reactions. The similar ionization rate enables a realistic contribution of ions into the whole ion-neutral coupled chemical network.

Tholins sample production: In order to recover the soluble part of the Titan's haze analog, 4 mg of tholins are dissolved in 1 ml of methanol in a vial. The vial is then vigorously stirred for 3 minutes to solubilize the maximum of species. The brown mixture is then filtered using a 0.2 μm polytetrafluoroethylene (PTFE) membrane filter on a filter holder. The filtered solution is transferred into a vial for future analyses and the insoluble fraction is recovered directly from the filter. The insoluble fraction in then dried in a glove box under inert atmosphere for few hours.

Scanning probe sample preparation: The Cu(111) single crystal was cleaned by repeated Ne^+ sputtering and annealing cycles. Bilayer NaCl islands were grown by evaporating NaCl onto the clean Cu(111) held at 273 K. Bulk tholins were sublimed in situ from a silicon wafer onto the substrate held at $\sim$10 K. CO for tip functionalization was dosed onto the substrate held at $\sim$10 K by admitting CO into the UHV system through a leak valve. Nitrogen-containing model compounds adenine, 1-aminopyrene, benz[*a*]acridine and 11H-benzo[*a*] carbazole were purchased from Sigma-Aldrich.

Atomic force microscopy: AFM experiments were carried out in a home-built, combined atomic force microscope/

scanning tunneling microscope, operated in UHV (base pressure $\sim 1 \times 10^{-10}$ mbar) and at low temperature ($\sim$5 K). AFM measurements were performed with a qPlus quartz force sensor (Giessibl 1998) operated in the frequency-modulation mode (Albrecht et al. 1991). The qPlus sensor had a resonance frequency of $\sim$28.8 kHz, quality factor of $\sim$100,000, and was operated at an oscillation amplitude $A = 50$ pm. All AFM images were acquired in the constant height mode at 0 V bias voltage with a CO-functionalized tip. To facilitate structure assignment, several AFM images at different tip-molecule distances where acquired for a given molecule (see Figures A4 and A5 in the Appendix).

We thank R. Allenspach for discussions. This work was supported by the ERC Consolidator Grant AMSEL (grant agreement 682144) and the European FET-OPEN project SPRING (grant agreement 863098); at COBRA Laboratory, by the European Regional Development Fund (ERDF) N° HN0001343, the European Union's Horizon 2020 Research Infrastructures program (Grant Agreement 731077), the Région Normandie, and the Laboratoire d'Excellence (LabEx) SynOrg (ANR-11-LABX-0029). N.C. thanks the European Research Council for funding via the ERC PrimChem project (grant agreement 636829).

Author Contributions

J.M., I.S.-A., T.G., C.A., and N.C. synthesized the Titan's haze analogs, F.S., K.K., L.G. and J.M. performed the AFM measurements. All authors contributed to analysis and discussion of the data and writing of the manuscript.

Appendix
Supporting Information

A.1. AFM Signatures of N-containing Model Compounds

Detailed structure assignment of unknown molecules on the basis of high-resolution AFM images can benefit from studies of known model compounds. These are used to characterize the AFM contrast of specific chemical moieties under different imaging conditions (e.g., different substrates, adsorption sites, tip heights, tip functionalizations) and subsequently identify them in a priori unknown molecules. Model compounds containing different linear alkyl chains and cycloaliphatic moieties were studied in detail previously (Schuler et al. 2017b). There are also some studies regarding the AFM image contrast of different heteroatoms in polycyclic hydrocarbons (Ellner et al. 2017; Gross et al. 2010; Kawai et al. 2018; Kocic et al. 2016; van der Heijden et al. 2016; Zahl & Zhang 2019).

In contrast to the previous molecular mixtures that were studied by high-resolution AFM (Commodo et al. 2019; Fatayer et al. 2018; Schuler et al. 2015; Schulz et al. 2019), Titan's haze laboratory analogs contain a large amount of nitrogen heteroatoms. Moreover, based on the molecule synthesis, nitrogen should be the only heteroatom present. However, the number and relative amount of nitrogen atoms can vary between individual molecules, and the nitrogen atoms can have different chemical environments. Therefore, we studied a set of model compounds with different N-containing moieties and different numbers of nitrogen atoms in various chemical environments to facilitate the structure assignment for our measurements. The different model compounds and their AFM images are shown in Figure A2.

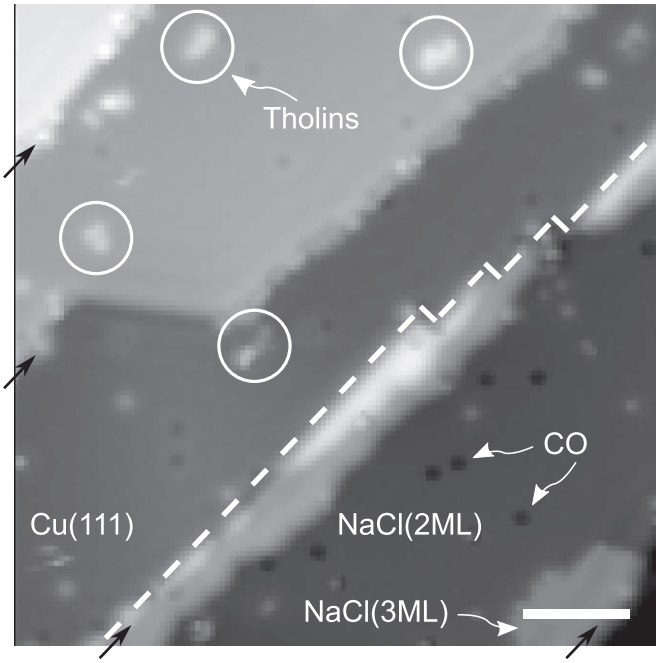

Figure A1. Typical constant-current STM overview image of the NaCl(2ML)/Cu(111) sample. The white dashed line indicates the edge of a bilayer NaCl island on the right-hand side. A small island of trilayer NaCl, CO molecules and some Titan's haze analogs (white circles) are marked as well. The black arrows indicate monatomic steps of the underlying Cu(111) surface. Tunneling setpoint: 0.2 V, 0.5 pA. Scale bar is 5 nm.

First, we studied three model compounds, each containing only one nitrogen but in different chemical environments, either as amine (1-Aminopyrene, AP), pyridine (Benz[*a*]acridine, BAA) (see also pyridine and pyrazine moieties measured by Kocic et al. 2016) or pyrrole (11H-Benzo[*a*]carbazole; BAC). The AFM images show that for each molecule, the part containing the nitrogen appears darker, indicating less repulsive interaction compared to the carbon backbone of the molecule. The dark contrast of the nitrogen sites is explained by a locally reduced adsorption height indicating that the nitrogen interacts stronger than carbon with the surface, resulting in a tilted adsorption geometry with N being closer to the surface compared to the remaining carbon backbone. In a recent study it was found that upon annealing the nitrogen sites in pyridine and pyrazine can bind metal adatoms (Kocic et al. 2016). As we prepared molecules at a sample temperature of $T = 10$ K and no annealing was performed, we can exclude the possibility of metal adatoms.

Importantly, the larger electronegativity of nitrogen compared to carbon results in a different electron density above the atomic species and slightly polar *C–N* bonds, which is relevant for the apparent distortions in AFM imaging (Ellner et al. 2017; Hapala et al. 2014; Kocic et al. 2016). The images for AP, BAA, and BAC in Figure A2 show molecules adsorbed on bilayer NaCl islands. We find similar images for these molecules on Cu(111).

Finally, we studied a model compound with a larger N/C ratio to qualitatively assess how the presence of several nitrogen atoms affects the adsorption behavior. In AP, BAA, and BAC the adsorption is governed by the single nitrogen forming a chemical bond with the surface resulting in a tilted adsorption geometry. In a molecule containing several N atoms, these will compete to form a bond with the surface. Adenine (AD) contains five nitrogen atoms in different chemical environments and it

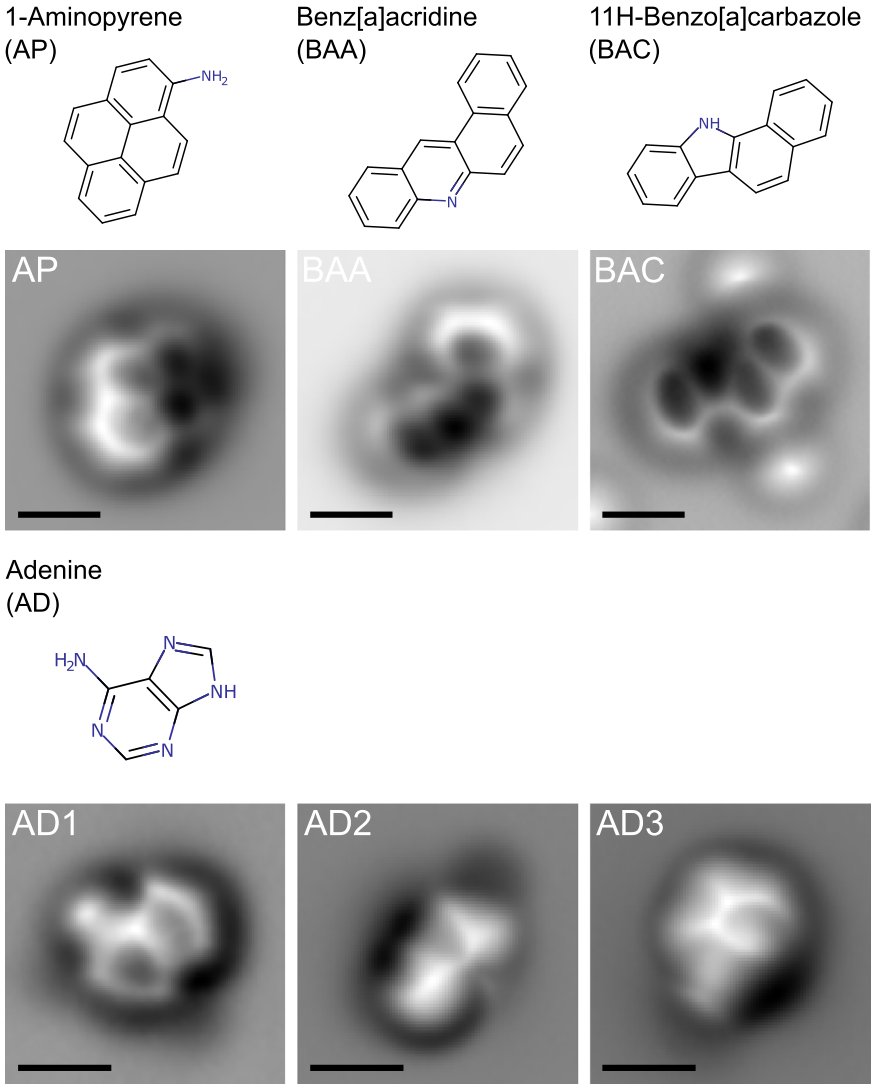

Figure A2. Molecular structure models and AFM images of nitrogen-containing model compounds. Images of AP, BAA, and BAC are acquired on NaCl(2ML)/Cu (111). Image AD1 is acquired on Cu(111) and AD2, AD3 on NaCl(2ML)/Cu(111). The two bright features adjacent to the molecule in the image of BAC are two CO molecules adsorbed on the NaCl film. All scale bars are 5 Ångström.

was previously identified in Titan's haze analogs (Horst et al. 2012). From our AFM study, we find several different adsorption geometries of AD, both on Cu(111) and NaCl (2ML)/Cu(111), three of which are shown in Figure A2. For some molecules, such as depicted in AD1, the uniform AFM contrast on the entire molecule indicates a relatively planar adsorption geometry. Other adsorption geometries in which the molecule is adsorbed in a tilted geometry indicate that only one or two nitrogen atoms on one site of the molecule form a chemical bond to the surface (see AD2 and AD3). In the planar adsorption geometry (AD1), the backbone of AD can be readily identified. Two important observations can be made. First, the presence of several N atoms within a heterocycle can lead to significant distortions in the AFM images, highlighted by the six-member ring of AD (lower part of the molecule in AD1) appearing almost triangular shaped. A similar contrast was predicted in a theoretical study of the AFM contrast (Ellner et al. 2017) and can be ascribed to the redistribution of electron density due to the nitrogen heteroatoms and its effect on the CO tilting (Ellner et al. 2017; Hapala et al. 2014; Kocic et al. 2016). Second, in this planar adsorption geometry the nitrogen atoms usually appear slightly brighter than the neighboring carbon atoms. In the AFM images of AD, BAA, and BAC, the N and NH groups within the heterocycle have a very similar contrast, demonstrating that these two groups are difficult to differentiate in the images of unknown molecules. This is similar for C and CH groups at the periphery of a PAH, where the absence of a hydrogen in the plane of the PAH is very challenging to be resolved (Majzik et al. 2018; Schuler et al. 2016). In the proposed tholin structures, N and NH groups are tentatively assigned such that the number of unpaired pi-electrons is minimal. However, even under these constrictions the assignment of N and NH is not always unique (see Figure A3 and Supporting Discussion).

A.2. Assignment of N and NH

The AFM images of the model compounds in Figure A2 indicate that N and NH groups within the heterocycle have a very similar contrast, demonstrating that these two groups are difficult to differentiate in the images of unknown molecules. In the proposed structures of the main text, N and NH groups were tentatively assigned such that the number of unpaired

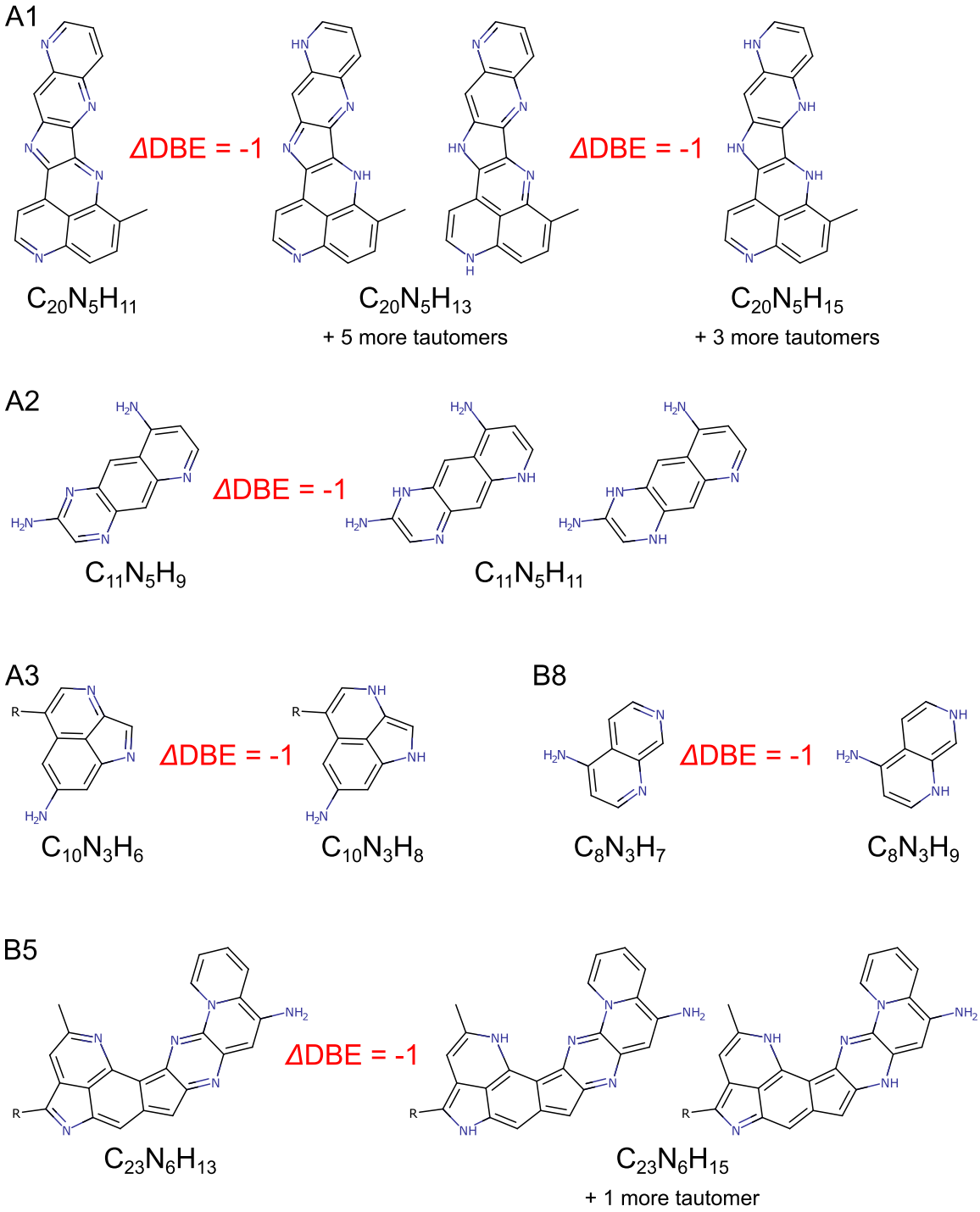

Figure A3. Alternative assignments of N and NH for the proposed molecular structures. The according differences in DBE are indicated as well.

pi-electrons is minimal. However, even under these constrictions the assignment of N and NH is not always unique. If more than one peripheral N/NH is present in the structure, different hydrogen tautomers may be possible, i.e., the molecular formula is the same, but the structure is different. In addition, in some cases the ratio between N and NH can be changed without introducing unpaired pi-electrons, i.e., also the molecular formula differs. Figure A3 summarizes the different structures and formulas for the molecules for which alternative assignments for N and NH are possible. Note that in some cases, not all hydrogen tautomers that could be possible based on the number of N atoms are reasonable, because of additional constraints such as side groups, aliphatic carbons or the connectivity of the backbone.

A.3. Additional STM and AFM Data

For the assigned molecules, we considered also the STM data and AFM images at different tip height, shown in Figures A4 and A5. Often the evolution of the AFM contrast as a function of tip height serves as a characteristic fingerprint for a specific moiety (Schuler et al. 2017b).

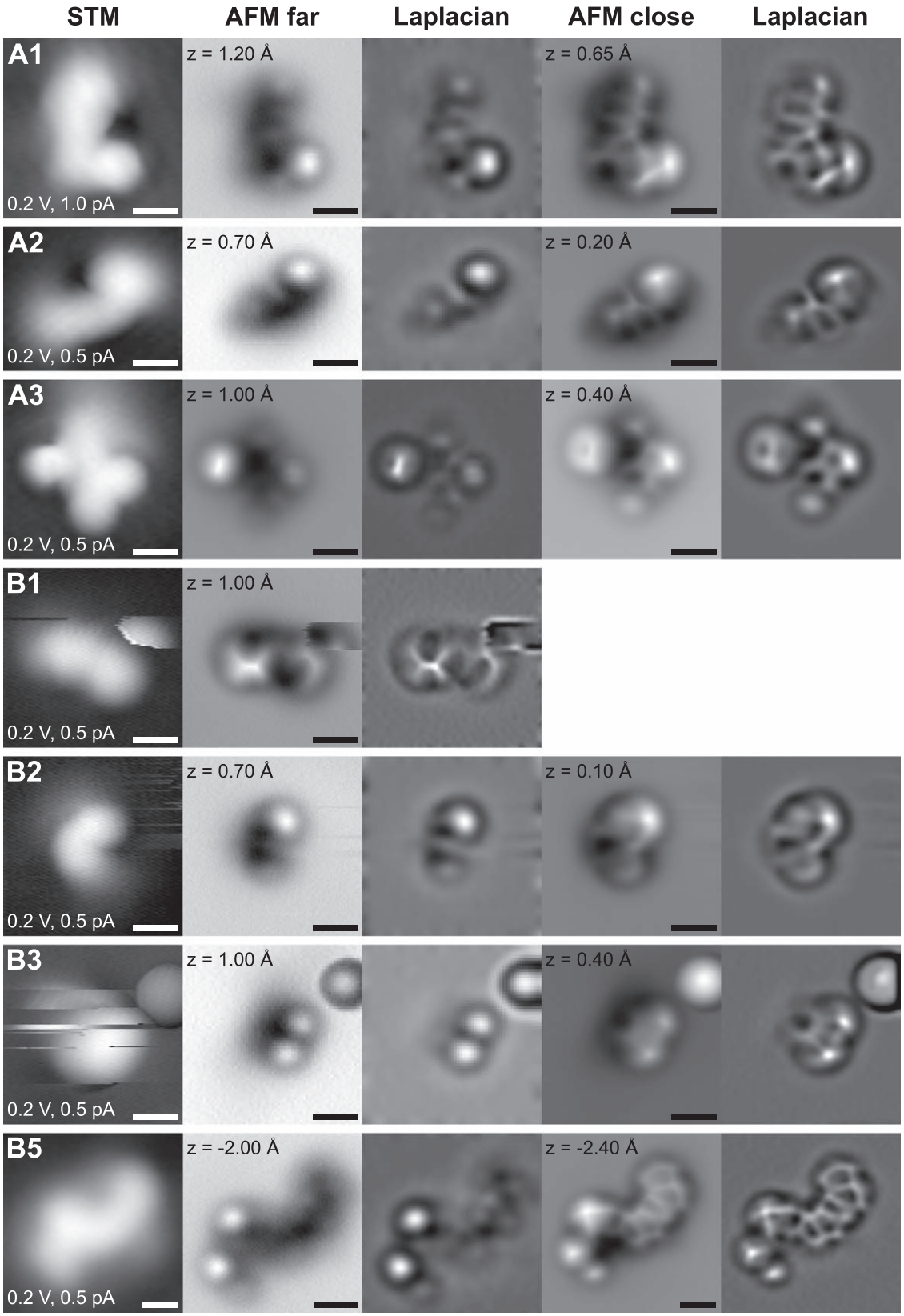

Figure A4. Additional STM and AFM data of assigned molecules. First column (STM): STM measurements in constant-current mode at indicated sample voltage V and tunneling current I. Second column (AFM far): const.-height AFM data. The tip-height offset with respect to the STM setpoint above the bare surface is indicated by z, where positive z corresponds to a increase in tip height. Third column: edge-enhanced (Laplace filtered) image of the second column. Fourth column (AFM close): AFM data at decreased tip height with respect to the second column. Fifth column: Laplace filtered image of the fourth column. All scale bars are 5 Ångström. Horizontal stripes in B1 and B3 result from changes in the molecular adsorption site under the influence of the scanning tip.

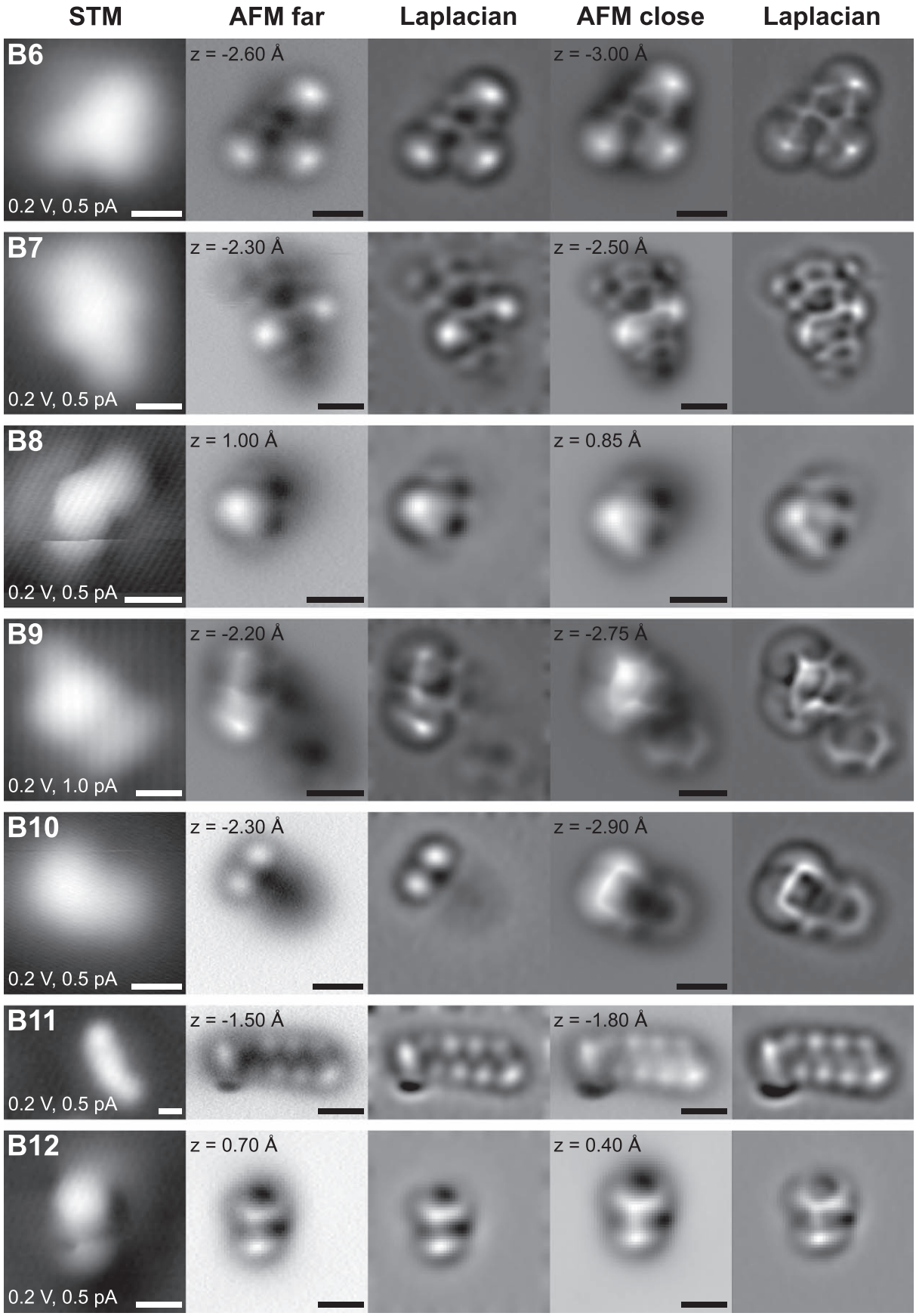

Figure A5. Additional STM and AFM data of assigned molecules. First column (STM): STM measurements in constant-current mode at indicated sample voltage V and tunneling current *I*. Second column (AFM far): const.-height AFM data. The tip-height offset with respect to the STM setpoint above the bare surface is indicated by z, where positive z corresponds to an increase in tip height. Third column: edge-enhanced (Laplace filtered) image of the second column. Fourth column (AFM close): AFM data at decreased tip height with respect to the second column. Fifth column: Laplace filtered image of the fourth column. All scale bars are 5 Ångström.

ORCID iDs

Fabian Schulz https://orcid.org/0000-0002-1359-4675
Julien Maillard https://orcid.org/0000-0001-5620-8474
Isabelle Schmitz-Afonso https://orcid.org/0000-0003-0665-0074
Carlos Afonso https://orcid.org/0000-0002-2406-5664
Nathalie Carrasco https://orcid.org/0000-0002-0596-6336
Leo Gross https://orcid.org/0000-0002-5337-4159

References

Albrecht, T. R., Grütter, P., Horne, D., & Rugar, D. 1991, JAP, 69, 668
Alldritt, B., Hapala, P., Oinonen, N., et al. 2020, SciA, 6, 6913
Atreya, S. K. 2007, Sci, 316, 843
Beuhler, R. J., Flanigan, E., Greene, L. J., & Friedman, L. 1974, JAChS, 96, 3990
Brassé, C., Muñoz, O., Coll, P., & Raulin, F. 2015, P&SS, 109, 159
Coates, A. J., Crary, F. J., Lewis, G. R., et al. 2007, GeoRL, 34, L22103
Coll, P., Navarro-González, R., Szopa, C., et al. 2013, P&SS, 77, 91
Commodo, M., Kaiser, K., De Falco, G., et al. 2019, CoFl, 205, 154
Cordier, D., & Carrasco, N. 2019, NatGe, 12, 315
de Oteyza, D. G., Gorman, P., Chen, Y.-C., et al. 2013, Sci, 340, 1434
Derenne, S., Coelho, C., Anquetil, C., et al. 2012, Icar, 221, 844
Dinelli, B. M., López-Puertas, M., Adriani, A., et al. 2013, GeoRL, 40, 1489
Ellner, M., Pou, P., & Pérez, R. 2017, PhRvB, 96, 075418
Fatayer, S., Albrecht, F., Zhang, Y., et al. 2019, Sci, 365, 142
Fatayer, S., Poddar, N. B., Quiroga, S., et al. 2018, JAChS, 140, 8156
Gautier, T., Carrasco, N., Buch, A., et al. 2011, Icar, 213, 625
Gautier, T., Schmitz-Afonso, I., Touboul, D., et al. 2016, Icar, 275, 259
Gautier, T., Sebree, J. A., Li, X., et al. 2017, P&SS, 140, 27
Giessibl, F. J. 1998, ApPhL, 73, 3956
Gross, L., Mohn, F., Moll, N., et al. 2010, NatCh, 2, 821
Gross, L., Mohn, F., Moll, N., et al. 2012, Sci, 337, 1326
Gross, L., Mohn, F., Moll, N., Liljeroth, P., & Meyer, G. 2009, Sci, 325, 1110
Gross, L., Schuler, B., Pavliček, N., et al. 2018, Angew. Chem., 57, 3888
Hamalainen, S. K., van der Heijden, N., van der Lit, J., et al. 2014, PhRvL, 113, 186102
Hapala, P., Kichin, G., Wagner, C., et al. 2014, PhRvB, 90, 085421
He, C., Hörst, S. M., Riemer, S., et al. 2017, ApJ, 841, L31
He, C., & Smith, M. A. 2014, Icar, 238, 86
Horst, S. M., Yelle, R.V., Buch, A., et al. 2012, AsBio, 12, 809
Hsu, C. S., Lobodin, V. V., Rodgers, R. P., McKenna, A. M., & Marshall, A. G. 2011, Energy Fuels, 25, 2174
Imanaka, H., Khare, B. N., Elsila, J. E., et al. 2004, Icar, 168, 344
Israël, G., Szopa, C., Raulin, F., et al. 2005, Natur, 438, 796
Kawai, S., Nakatsuka, S., Hatakeyama, T., et al. 2018, SciA, 4, eaar7181
Kocic, N., Liu, X., Chen, S., et al. 2016, JAChS, 138, 5585
Lavvas, P., Yelle, R. V., Koskinen, T., et al. 2013, PNAS, 110, 2729
López-Puertas, M., Dinelli, B. M., Adriani, A., et al. 2013, ApJ, 770, 132
Mahjoub, A., Carrasco, N., Dahoo, P. R., et al. 2012, Icar, 221, 670
Mahjoub, A., Schwell, M., Carrasco, N., et al. 2016, P&SS, 131, 1
Maillard, J., Carrasco, N., Schmitz-Afonso, I., Gautier, T., & Afonso, C. 2018, E&PSL, 495, 185
Maillard, J., Hupin, S., Carrasco, N., et al. 2020, Icar, 340, 113627
Majzik, Z., Pavliček, N., Vilas-Varela, M., et al. 2018, NatCo, 9, 1198
McGuigan, M., Waite, J. H., Imanaka, H., & Sacks, R. D. 2006, JCh, 1132, 280
Moll, N., Gross, L., Mohn, F., Curioni, A., & Meyer, G. 2010, NJPh, 12, 125020
Pavliček, N., Fleury, B., Neu, M., et al. 2012, PhRvL, 108, 086101
Pavlov, A. A., Brown, L. L., & Kasting, J. F. 2001, JGR, 106, 23267
Rapenne, G., Grill, L., Zambelli, T., et al. 2006, CPL, 431, 219
Ruger, C. P., Maillard, J., Le Maître, J., et al. 2019, JASMS, 30, 1169
Schuler, B., Fatayer, S., Meyer, G., et al. 2017a, Energy Fuels, 31, 6856
Schuler, B., Fatayer, S., Mohn, F., et al. 2016, NatCh, 8, 220
Schuler, B., Meyer, G., Pena, D., Mullins, O. C., & Gross, L. 2015, JAChS, 137, 9870
Schuler, B., Zhang, Y., Collazos, S., et al. 2017b, Chem. Sci., 8, 2315
Schuler, B., Zhang, Y., Liu, F., et al. 2020, Energy Fuels, 34, 15082
Schulz, F., Commodo, M., Kaiser, K., et al. 2019, Proc. Combust. Inst., 37, 885
Sciamma-O'Brien, E., Ricketts, C. L., & Salama, F. 2014, Icar, 243, 325
Szopa, C., Cernogora, G., Boufendi, L., Correia, J. J., & Coll, P. 2006, P&SS, 54, 394
Trainer, M. G., Pavlov, A. A., DeWitt, H. L., et al. 2006, PNAS, 103, 18035
van der Heijden, N. J., Hapala, P., Rombouts, J. A., et al. 2016, ACS Nano, 10, 8517
Vinatier, S., Rannou, P., Anderson, C. M., et al. 2012, Icar, 219, 5
Vuitton, V., Yelle, R. V., & Anicich, V. G. 2006, ApJ, 647, L175
Waite, J. H., Young, D. T., Cravens, T. E., et al. 2007, Sci, 316, 870
Yoon, Y. H., Hörst, S. M., Hicks, R. K., et al. 2014, Icar, 233, 233
Yu, X., Hörst, S. M., He, C., et al. 2020, ApJ, 905, 88
Zahl, P., & Zhang, Y. 2019, Energy Fuels, 33, 4775
Zhang, Y., Schuler, B., Fatayer, S., et al. 2018, Ind. Eng. Chem. Res., 57, 15935